P2.7 THE IMPACT OF DOPPLER RADAR DATA ON RAINFALL FORECAST: A CASE STUDY OF A CONVECTIVE RAINBAND EVENT IN MISSISSIPPI DELTA USING WRF 3DVAR

Eunha Lim[1*], Qingnong Xiao[1], Juanzhen Sun[1],
Patrick J. Fitzpatrick[2], Yongzuo Li[2], Jamie Dyer[3], and Dale M. Barker[1]

[1] National Center for Atmospheric Research* Boulder, Colorado
[2] GeoResources Institute, Mississippi State University, Stennis Space Center, Mississippi
[3] Department of Geosciences, Mississippi State University, Starkville, Mississippi

1. Introduction

The improvement of short-term rainfall forecast using numerical models has been vigorously pursued during the last decade. One of the approaches to improve rainfall prediction for mesoscale and convective-scale is to produce initial conditions closer to true fields by assimilating radar observations using advanced data assimilation techniques.

There are three dominant approaches to improve model initial conditions using Doppler radar volumetric data. They are three- and four-dimensional variational (3DVar, 4DVar) data assimilations, and ensemble Kalman Filter (EnKF). The 4DVar technique was first applied to radar data assimilation by Sun et al. (1991). In recent years, it has been shown that the technique is able to retrieve the 3D wind, thermodynamic, and microphysical variables and improve subsequent precipitation forecasting (Sun and Crook 1997, 1998; Sun 2005). The EnKF technique is a newer technique and has been applied to radar data assimilation (Snyder and Zhang 2003, Dowell et al. 2004, and Tong et al. 2006). While both the 4DVar and EnKF were demonstrated the capability of retrieving the unobserved model variables through the use of a dynamical model, they are computationally too expensive to be applied in real time with a large domain. Xiao et al. (2005, 2007), therefore, developed a radar radial velocity and reflectivity data assimilation procedure in MM5 3DVar system (Barker et al. 2003) and examined its capability in two case studies. They showed that rainfall forecasts were improved with a 3-hour analysis/forecast update cycling system when verified against observation. Hu et al. (2006) assimilated reflectivity and radial velocity using a different procedure based on the 3DVar system for the Advanced Regional Prediction System (ARPS) in a case study of tornadic thunderstorm forecasting.

Although the 3DVar technique has been shown some success in radar data assimilation through a few case studies, there are still a host of unresolved questions. One prominent question concerns the background error statistics for mesoscale applications. In this paper, we want to address the question in regard to forecast length when ensemble-based forecast are used to produce background error statistics. We applied random perturbation technique (Barker 2005) in Weather Research and Forecasting (WRF) 3DVar to calculate background error covariance for a band-type rainfall event in Mississippi delta during 29-30 April 2005. The impact of the error statistics produced by 3-, 6-, and 12-hour ensemble forecasts were compared on the subsequent precipitation forecasts. We then used the statistics that produced the best forecasts to run several experiments to examine the impact of the 3DVar with radar data and cycling. This paper is arranged as follows. Section 2 describes the ensemble-based background error statistics method, its characteristics and impact on forecast. Radar data pre-processing are described in section 3. Section 4 presents the experimental results of radar data assimilations and their evaluation in the rainfall forecasts. This paper concludes with summary in section 5.

2. Ensemble-based background error statistics and its characteristics

We adopted the ensemble-based background error statistics method (Fisher 1999) to calculate background error covariance for the case. Random perturbations were generated in control variables of WRF 3DVar and the ensemble forecast is produced with the WRF model integration. The center of the model domain is (33.5°N, 90.0°W) in the state of Mississippi. The grid mesh is 350×350×35 with 4 km horizontal resolution. The model top is set 50 hPa. The control initial condition is interpolated from Eta reanalysis data that has about 40 km horizontal

---

* *Corresponding author address*: Eunha Lim, NCAR/RAL Division, P.O. Box 3000, Boulder, CO 80307-3000; e-mail: lim@ucar.edu

resolution (we will call it the control member hereafter). The model integration time step is 24 seconds.

a. Generation of ensemble initial conditions

We assume the error in the initial conditions can be represented by random perturbation that has Gaussian distribution with zero mean and unit standard deviation in the control variable space of WRF 3DVar. It is incremental formulation of control variables (v) in a model space. The control variables in WRF 3DVar are stream function, unbalanced velocity potential, unbalanced temperature, pseudo relative humidity, and unbalanced surface pressure. Background error covariance is described in the space of uncorrelated control variables to decrease the computational expense of the cost function. The horizontal and vertical correlations between model variables (x) are introduced via control variable transform which includes recursive filter in the horizontal, empirical orthogonal function projection (EOF) in the vertical, and some physical balances of hydrostatic, geostrophic, and cyclostrophic relations (Barker et al. 2003).

The final analysis increments of model variables are three-dimensional, multivariate fields with spatial correlations. The 30 ensemble initial conditions are generated using different random seeds. Each ensemble initial condition is constructed by adding the increment field to the field of control member. The boundary condition with 3-hr interval for each ensemble member is updated by perturbed analysis field to prevent an ensemble forecast from losing variance as lead time increases.

b. Characteristics of background error statistics

To analyze the characteristics of ensemble-based background error statistics, we calculated the ensemble forecasts from 0000 UTC 30 April 2005 for the case. Each ensemble forecast member integrated 12 hours, and the background error statistics were carried out from the forecasts at 3, 6, and 12 hours, respectively. The background error is defined as the perturbation from the ensemble mean.

Figure 1 shows the correlation between total value and the balanced value with stream function for temperature (a) and velocity potential (b) with respect to forecast time. The mass and wind correlation increases as forecast proceeds (Figure 1a). It implies that forecast model smoothes the smaller scale structures as lead time increases. However, the overall magnitude

of correlations is smaller than 0.2; 80 percent of temperature leaves for unbalanced with wind. The correlation in velocity potential (Figure 1b) varies in levels as well as in time. The correlation at 12-hour ensemble forecast has maximum in the lower levels, while 6-hour ensemble correlations has maximum in the mid-lower levels. The correlations from 3-hour ensemble forecasts are the smallest among the three ensemble forecasts in all levels.
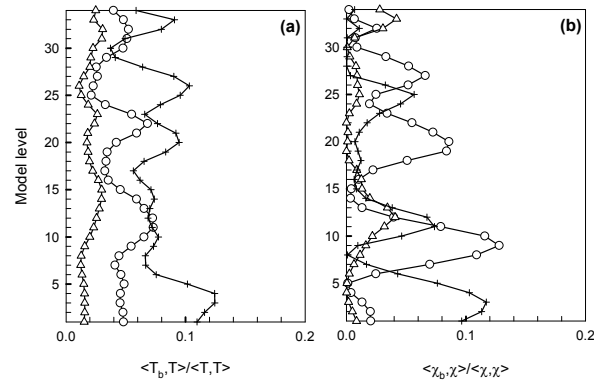

Figure 1. Vertical profiles of correlations between balanced and total value of temperature (a), velocity potential (b) for different forecast times. Triangle, circle, and cross stand for 3-, 6-, and 12-hour forecast, respectively.

The horizontal scale length of background error determines the influence of observations and smoothness of each observation. Figure 2 shows scale lengths of all control variables for three different background errors. In general, the length scales of all control variables are increased along with the increase of the ensemble forecast time. Temperature and relative humidity (Figure 2c and d) have similar length scales; both show the nature of smaller scale than wind, i.e. stream function and unbalanced velocity potential (Figure 2a and b).

The magnitude of background error is represented by the eigenvalue from the background error covariance matrix. The background error of unbalanced velocity potential is about 40 percent of stream function. The error of background temperature is about 3.4 ^{o}K for the first mode when 12-hour ensemble forecasts are used. It is within the range of temperature observation error defined by NCEP. The temperature errors for 3- and 6- hour forecast are out of the observation error range. It suggests that temperature observation plays a relatively dominant role when 3-hour ensemble forecasts are used for the background error statistics. The temperature error decreases rapidly after the first

mode. The background errors of relative humidity among three ensemble forecasts are not significantly different.
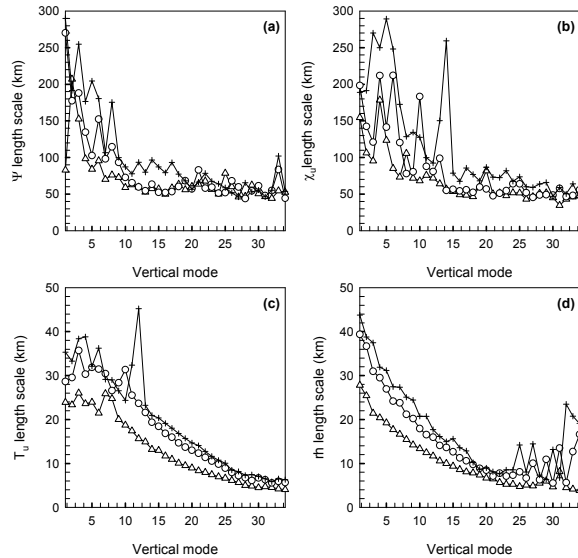

Figure 2. Horizontal length scales of background error for stream function (a), unbalanced velocity potential (b), unbalanced temperature (c), and relative humidity (d). Symbol notations are the same as those in Figure 1.

3. Radar data processing

The quality of the observational data plays a crucial role in the results of data assimilation. There are two main issues for radial velocity quality control. Doppler radar observes radial velocity within the range of unambiguous velocity. The velocity is folded where true wind is greater than the unambiguous velocity; it has to be unfolded. Radar displacement is not homogeneous. It induces not only data void area but data overlapped area from several radars in the network. Even if one radar is considered, it is usually too dense compared with the horizontal resolution of numerical models. Data thinning or super-observation strategy is necessary.

There are several stages to process radar data before ingesting to WRF 3DVar for this study. First, radial spherical coordinates are converted to the two-dimensional Cartesian coordinates with a 1 km grid interval on each constant-elevation-angle surface. Second, folded radial velocities are unfolded using wind profile, extracted from the WRF initial fields, as a reference wind. The next stage is to remove radial velocities, which are smaller than 0.1 ms^{-1} to eliminate ground-clutter contamination. Further quality control is achieved by a generalized procedure to remove noisy data. In particular, a local variance is computed, and any data point

with a variation of greater than 60.0 m^{2}s^{-2} is removed. A 2-dimensional filter that is based on a local least-squares fitting method is then applied to remove high frequency features that cannot be adequately represented by the model grid. The next step is to horizontally interpolate the 1 km data to 4 km, which is WRF model grid for this study, while still keeping the data on constant-elevation-angle surfaces. The standard deviation of data, which are involved in the interpolation, is used as an observation error in the variational analysis. The above processes are applied for nine radars separately. The final step is to make a super observation data with about 20 km resolution. If there are several profiles of data from different radars in 20×20 km^2 area, we select one profile with the following criteria in order: more data in the vertical, and shorter distance from the radar.

Figure 3 shows the radial velocities before and after the quality control procedure for the site KNQA on 2.3-degree elevation angle at 00UTC 30 April 2005. The horizontal resolutions are 1 and 4 km, respectively. There are folded velocities at northeast and southwest edge of the data area (Figure 3a). They show strong contrast between away and toward wind. The radial winds are unfolded as shown in Figure 3b.
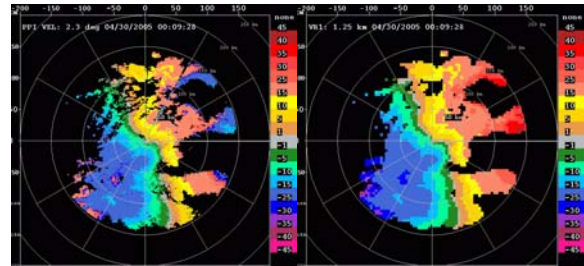

Figure 3. Observed (left) and unfolded (right) radial velocities on 2.3 deg elevation angle for NEXRAD KNQA at 00 UTC 30 April 2005.

4. Results

Nine experiments were designed (Table 1) to address the three subjects. One is to select the proper background error covariance for the rainfall events. Experiments BE03, BE06 and GTS are conducted mainly for this purpose. The experiments CNTL, GTS and RADR are to analyze the impact of radar data assimilation on the forecasts of the rainfall event, especially for the initiation of new convective cells at 06 UTC 30 April 2005. The experiment RADR_nt is designed to compare with RADR in terms of impact of radar data thinning. The other three experiments with prefix C are designed to assess

the impact of the analysis and forecast cycling. In addition to model configuration mentioned in section 2, the main model physics used in this study include the WRF-Single-Moment 6-class graupel scheme (WSM6, Hong and Lim 2006),

Rapid Radiative Transfer Model (RRTM, Mlawer et al, 1997), Dudhia scheme (Dudhia 1989) for long and short radiations, and YSU planetary boundary layer parameterization scheme (Hong et al. 2006).

Table 1. Experimental design.

Experiment	Background error time (hours)	Forecast time (UTC)		Data		Remarks
		Start	End	GTS	Radar	
CNTL	-	3000	3012	No	No	
BE03	3	3000	3012	Yes	No	
BE06	6	3000	3012	Yes	No	
GTS	12	3000	3012	Yes	No	
RADR_nt	12	3000	3012	Yes	Yes	no thinning
RADR	12	3000	3012	Yes	Yes	
C_CNTL	12	2918	3012	No	No	
C_GTS	12	2918	3012	Yes	No	
C_RADR	12	2918	3012	Yes	Yes	

a. Impact of different background error covariance

To determine the most appropriate background error covariance for the rainfall event, we carried out three experiments BE03, BE06, and GTS with 12-hour forecast using only conventional observations from Global Telecommunication System (GTS) in the 3DVar analyses. The performance of each background error covariance is evaluated by three-hour accumulated rainfall verification. Figure 4 shows equitable threat score (ETS) and bias from the rainfall forecast of each experiment. For lighter rain with threshold of 0.1 mm (Figure 4a), the background error covariance calculated from 12-hour ensemble forecast has the highest ETS. Relative large length scale, which results in wider influence of observation by the background error statistics, could be a reason for the highest ETS. Biases of three experiments for light rainfall are close to 1, but they all increases at later forecast time.

For heavier rainfall with threshold of 2.5 mm, GTS produces better ETSs at all forecast time (Figure 4b) except for 9-hour forecast. The biases of BE06 and GTS are similar, and both are slightly larger than that of BE03. The rainfall verification from this study indicates that model needs spin-up time to produce heavier rainfall. There is no significant superiority of using any one of the background error covariance (from 3, 6 or 12 ensemble forecast) in terms of rainfall verification. With the background error statistics from 12-hour ensemble forecast, however, the average ETS shows a little higher score than using other two. In the following experiments we used the background error covariance from 12-hour

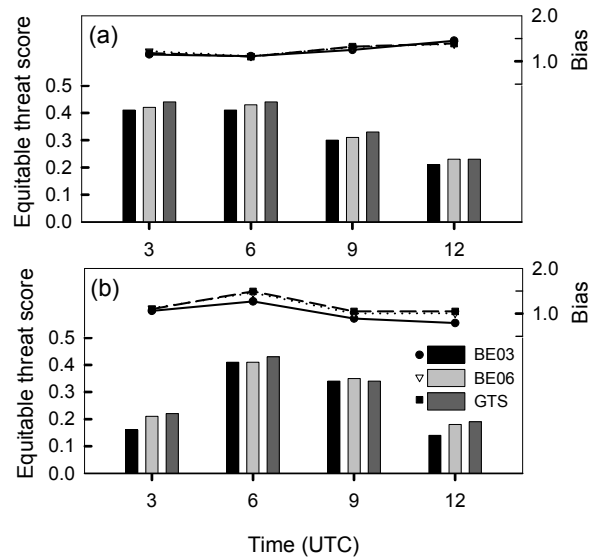ensemble forecast to evaluate the impact of radar data assimilation.

Figure 4. Equitable threat score (bar) and bias (line with symbol) of 3-hour accumulated rainfall for experiments, BE03, BE06, and GTS with 0.1 (a) and 2.5 mm (b) threshold at 30 April 2005.

b. Impact of radar data assimilation

The analysis increment at 1000 hPa from the experiment GTS is shown in Figure 5a. Assimilation of the conventional data increases the moisture mainly around the coast of Texas, Louisiana, and Mississippi. There is a moisture intrusion from the coast, stretching in the cold front direction (Figure 5a and c). Temperature decreases behind the cold front and increases in the warm region. Figure 5b and d are the

differences of wind analysis increments between RADR and GTS at 1000 and 850 hPa, respectively. Assimilation of radial velocities increases not only the southwesterly wind in front of the cold front at 1000 hPa, but northwesterly wind behind the cold front.
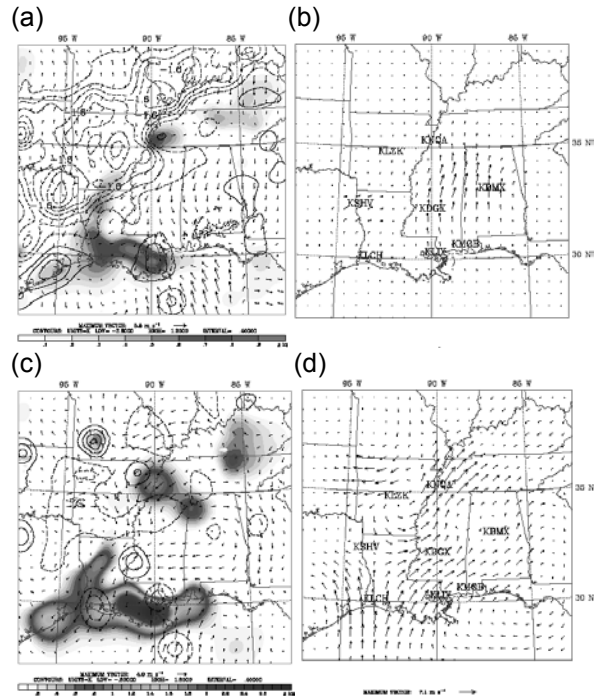
(a)   (b)

(c)   (d)

Figure 5. Analysis increments of temperature (contour, interval = 0.4 °K, dashed line stands for negative), specific humidity (shaded, unit = g kg^{-1}) and wind vector for GTS (left panel), and analysis increment difference of RADR from GTS (right panel) at 1000 (upper) and 850 hPa (lower). The names in the right panel stand for radar locations assimilated in the experiment RADR.

Figure 6 shows the 3-hour accumulated rainfalls at 06 UTC 30 April 2005. Figure 6a is the observation. There are several convective cells embedded in the existing rain band associated with the cold front. A new storm initiated at 06 UTC in front of the existing rain band in southern Louisiana. It gradually developed into a rain band and moved northeastward in later time. The rain band in CNTL (Figure 6b) encompasses the storm cells and stretches to Texas where the observation does not have it. It also does not have straight shape; it is kinked around the border of Mississippi, Arkansas, and Louisiana. Conventional data assimilation (GTS) helps the rain band get straight shape at 06 UTC (Figure 6c). Radial velocity assimilation (RADR) helps the generation of the new storm in front of the rain

band, but it is developed at the southwest of Louisiana (Figure 6d).

(a)   (b)
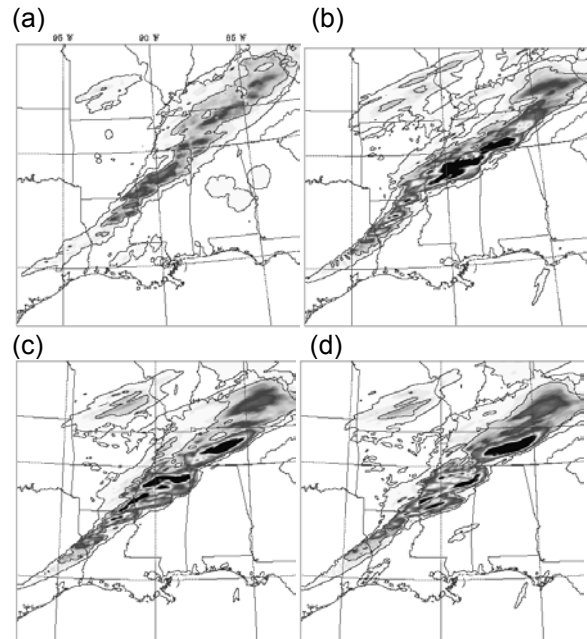
(c)   (d)

Figure 6. 3-hour accumulated rainfall 06 UTC 30 April 2005 for observation (a), CNTL (b), GTS (c), and RADR(d). The two contours are drawn at 0.1 mm and 2.5 mm.

The ETSs of 3-hour accumulated rainfall for experiments CNTL, GTS, and RADR are shown in Figure 7 with solid bars. Overall, 3DVar experiments that have conventional data and radar data assimilations produce better results in the rainfall forecasts than that without data assimilation (CNTL). For lighter rain (Figure 7a), GTS has higher ETS score than RADR for the first 6 hours, but RADR has better ETS skill than GTS after 6 hours. For heavier rainfall (figure 7b), the ETS from RADR is higher than GTS at all forecast time. Careful examination indicates that the improvement of RADR over GTS is mainly due to the catch-up of the new storm development around 06 UTC. Biases are similar for all experiments.

The thinned radar data (RADR) makes the 3DVar converge at 31 iterations. As a comparison, RADR_nt with original data makes 3DVar converge at 71 iterations. The 3DVar minimization of RADR is two times faster than RADR_nt. We should point out that with the reduced computation cost, we still obtained similar results in terms of ETS, bias, and horizontal distribution.
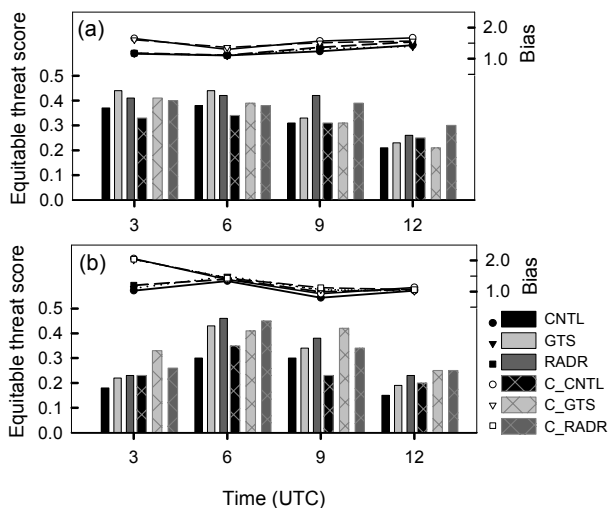
Figure 7. Equitable threat score (bar) and bias (solid line with symbol) of 3-hour accumulated rainfall for experiments, CNTL, GTS, and RADR with 0.1 (a) and 2.5 mm (b) threshold at 30 April 2005. Hatched bar and dashed line with symbols stand for equitable threat score and bias for experiments, C_CNTL, C_GTS, and C_RADR.

c. Impact of analysis and forecast cycling

Radar data are available from the 18 UTC 29 April, which is set as the cold start time for the 3DVAR cycling experiments. The frequency of the update cycles is 3 hours. We noticed that every cycling experiment increases the biases at 03 UTC but after that, biases are closer to those of no cycling experiments (Figure 7). C_CNTL produces worse results than CNTL in general for lighter rainfall (Figure 7a) and at 09 UTC for heavier rainfall (Figure 7b) in terms of ETS. The new storm cell in C_CNTL is developed further than that of CNTL. Two systems appear to merge together on later forecast time. It is the reason that C_CNTL has a higher ETS at 12 UTC than that of CNTL (Figure 7b).

C_GTS also does not produce higher ETS than that of GTS for lighter rainfall (Figure 7a), because it produces the lighter rainfall in wider area than that of GTS. It does not help the initiation of the new storm at 06 UTC; however, it produces the higher EST than that of GTS for heavier rainfall (Figure 7b). It is mainly due to keeping the strong convection at the trailing of the existing rain band.

Radar data cycling (C_RADR) generates the new storm, which is closer to the observation than RADR in terms of location and the size, even though it has narrower shape and a little bit northern place than observation. This results in the higher ETS than that of C_GTS in the lighter rain (Figure 7a). It is not intensified like an

observation. Radar data cycling intensifies the existing rain band at the boarder of Arkansas, Louisiana, and Mississippi. The feature is close to the observation, however, it does not simulate the merge of two systems.

5. Summary and conclusion

To assess the impact of Doppler radar data assimilation on short-term rainfall forecasts, WRF 3DVar analysis and WRF model forecast systems were applied to a convective rain band case in Mississippi Delta. The convective rain band occurred in association with a cold front on 29-30 April 2005 in the area.

The first effort in this study was to find an appropriate background error covariance for the case using ensemble forecasts. The ensemble initial conditions are generated by random perturbations in the control variable space using WRF 3DVar. Three background error covariance were calculated from 3, 6 and 12-hour ensemble forecasts initialized at 00 UTC 30 April 2005. Background error statistics showed that the balances between wind and mass were increased with the increase of forecast time. The horizontal correlation was also increased. Meanwhile the error magnitude of control variables is reduced, because the ensemble spread is reduced as forecast time increases. The performance of background error statistics were estimated based on ETS skills of 3-hour accumulated rainfall forecast. Although not significantly different, the background error covariance using 12-hour ensemble forecast produced the best results. This indicates that a longer time ensemble forecast establishes more balanced background structure, which produces better representative of the background error covariance.

The second effort was to evaluate how radar data assimilation helps improve the forecast of rain band in terms of generation of new storm. Radar data assimilation initiates the new storm in front of the existing rain band, although it is misplaced a little and not as strong as in the observation. We also investigated the impact of radar data thinning on the rainfall forecast. It is indicated that assimilation of the thinned radar data resulted in about two times faster converging during the 3DVar minimization, while produce similar ETS skills compared with the experiment without tinning.

Analysis and forecast cycling from 18 UTC 29 April 2005 were designed to address the importance of more data used in the data cycling window. In the series of experiments, radar and conventional GTS data are assimilated three

times until 0000 UTC 30 April 2005 with 3-hour intervals. Cycling with GTS data does not help to enhance the performance of forecast skill of lighter rainfall, but it increases the forecast performance for heavier rainfall by developing strong storms at the trailing of the existing rain band. Cycling with radar data initiated new storms closer to the observation than that without cycling. It also produces better evolution and propagation of the storm than non-cycling experiments. The ETS skills are therefore enhanced for lighter rainfall, especially at the later forecast time. However, there is no significant improvement of heavier rainfall forecast with only radial velocity assimilation.

Even though radar data assimilation had better performance to initiate new storm, there is still a main difference from the observation in propagations of the main rain band and the new storm. We should make more efforts to further improve the forecast of the rain band. In addition, the capability of Doppler radar data assimilation in WRF 3DVAR is under rapid improvement. We will include diabatic process related to radar reflectivity observation in the system. More positive impacts from Doppler radar data assimilation are expected in the future.

References

Barker, D. M., W. Huang, Y.-R. Guo, A. J. Brourgeois, and Q. N. Xiao, 2003: A three-dimensional variational data assimilation system for MM5: Implementation and initial results. *Mon. Wea. Rev.*, **132**, 897-914.

_____, 2005: Southern high-latitude ensemble data assimilation in the Antarctic mesoscale prediction system. *Mon. Wea. Rev.*, **132**, 3431-3449.

Dowell, C.D., F. Zhang, L.J. Wicker, C. Snyder, and N.A. Crook, 2004: Wind and temperatures in the 17 May 1981 Arcadia, Oklahoma, supercell: Ensemble Kalman filter experiments. *Mon. Wea. Rev.*, **132**, 1982-2005.

Dudhia, J., 1989: Numerical study of convection observed during the winter monsoon experiment using two-dimensional model. *J. Atmos. Sci.*, **46**, 3077-3107.

Fisher, M., 1999: Background error statistics derived from an ensemble of analysis. ECMWF Research Department Technical Memorandum, No. 79, 12pp.

Hong, S.-Y., Y. Noh, and J. Dudhia, 2006: A new vertical diffusion package with an explicit treatment of entrainment processes. *Mon. Wea. Rev.*, **134**, 2318-2341.

_____, and J.-O. J. Lim, 2006: The WRF single-moment microphysics scheme (WSM6). *J. Korean. Meteor. Soc.*, **42**, 129-151.

Hu, M., M. Xue, J. Gao, K. Brewster, 2006: 3DVAR and cloud analysis with WSR-88D level-II data for the prediction of the Fort Worth, Texas, tornadic thunderstorms. Part II: Impact of radial velocity analysis via 3DVAR. *Mon. Wea. Rev.*, **134**, 699-721.

Snyder, C., F. Zhang, 2003: Assimilation of simulated Doppler radar observation with an Ensemble Kalman filter. *Mon. Wea. Rev.*, **131**, 1663-1677.

Sun, J., D. Flicker, and D. Lilly, 1991: Recovery of three-dimensional and temperature fields from simulated single-Doppler Radar data. *J. Atmos. Sci.*, **48**, 876-890.

_____, and _____, 1997: Dynamical and microphysical retrieval from Doppler radar observation using a cloud model and its adjoint. Part I: Model development and simulated data experiments. *J. Atmos. Sci.*, **54**, 1642-1661.

_____, and _____, 1998: Dynamical and microphysical retrieval from Doppler radar observation using a cloud model and its adjoint. Part II: Retrieval experiments of an observed Florida convective storm. *J. Atmos. Sci.*, **55**, 835-852.

_____, 2005: Initialization and numerical forecasting of a supercell storm observed during STEPS. *Mon. Wea. Rev.*, **133**, 793-813.

Tong, N., M. Xue, and M. Hu , 2006: Assimilation of Radar Data for Thunderstorm Prediction with Ensemble Kalman Filter: A Real Case Study. *The Doug Lilly Symposium*, Atlanta, GA, Amer. Meteor. Soc.

Xiao, Q., Y.-H. Kuo, J. Sun, W.-C. Lee, E. Lim, Y.-R. Guo, D.M. Barker, 2005: Assimilation of Doppler radar observations with a regional 3DVAR system: Impact of Doppler velocities on forecasts of heavy rainfall case. *J. Appl. Meteorol.*, **44**, 768-788.

_____, _____, _____, _____, D.M. Barker, E. Lim, 2007: An approach of radar reflectivity data assimilation and its assessment with the inland QPF of typhoon RUSA (2002) at landfall. *J. Appl. Meteorol.*, **46**, 14-22.